Numerical Analysis of Freeway Traffic Flow Dynamics under Multiclass Drivers

Zuojin Zhu[1] , Gang-len Chang[2] and Tongqiang Wu[3]

[1] Department of Thermal Science and Energy Engineering, University of Science and Technology of China, Hefei, Anhui 230026, P.R. China. Email: zuojin@ustc.edu.cn, Fax: 86-551-3631760, Phone: 86-551-3603803.

[2] Professor, Department of Civil Engineering, University of Maryland, USA. Email: gang@Glue.umd.edu.

[3] PhD Candidate, Department of Operations Research and Financial Engineering, Princeton University, Princeton, NJ, 08540, USA. Email: twu@princeton.EDU

Abstract: This paper presents a first-order multi-class model for illustrating freeway traffic dynamics, especially regarding the temporal and spatial variation of both densities and flow rate along freeway segments without the disturbance from ramp flows. The proposed macroscopic model is grounded on the assumption that freeway traffic may consist of multiple classes of drivers who, charaterized with their unique speed –density relation, are likely to react differently under the same driving environment. The distribution of various classes of drivers and their differences in responding to perceived driving conditions may contribute significantly to the observed freeway traffic dynamics that remains to be better explained by existing traffic flow theories. The numerical solution and simulation results reported in this study, however, indicate that our proposed first-order multiclass model offers the potential to explore the complex interactions between freeway drivers and their collective impact on traffic flow patterns.

INTRODUCTION

Recognizing the limitations of the existing traffic flow theory, traffic researchers over the past several decades have devoted considerable efforts on developing a reliable model that can realistically capture the complex traffic flow dynamics. One of the primary research directions is to replace the first-order hydrodynamic traffic model with a high-order difference or differential system of equations. For example, Zhang (1) has presented a new continuum traffic theory and investigated its wave properties. Helbing *et al.* (2) have developed a traffic flow simulator, called MASTER, based on gas-kinetic traffic equations. They have also developed a new class of molecular-dynamics-like microscopic traffic models based on times to collisions (Helbing, *et al.*, (3)).

Some researchers in recent years have attempted to extend the high-order macroscopic model to incorporate multiclass drivers in traffic flow formulations. Examples of pioneering studies along this line are due to Nagatani (4) Hoogendoorn and Bovy (5). While the former have characterized the discrepancy between the car-following behavior of various types of drivers with their delay time, the latter has employed the gas-kinetic equations to model the multiclass traffic flow interactions. A concise review of research developments along this line can be found in the work of Kuhne and Michalopoulos (6).

Despite the significant progress on high-order macroscopic traffic flow models, their complex formulations and the number of parameters to be calibrated may degrade their potential for field applications. Thus, instead of developing high-order mathematical traffic relations, some researchers suggested that the effort should be devoted to capturing the discrepancy of driver behavior in a macroscopic model formulation (Daganzo, (7)). A simple fist-order mathematical model may be sufficient for capturing traffic flow dynamics if the response of different types of drivers and their collective impacts on the traffic conditions have been properly taken into account. An example of studies along this line can be found in a two-phase traffic flow model proposed recently by Zhu and Wu (8) in which the free-flow speed in a first-order macroscopic traffic model is assumed to vary across driving populations.

In fact, a recent empirical study by Cassidy and Mauch (9) has also concluded that under congested queued conditions, there exists a well–defined relation between the flow rate and the cumulated number of vehicles on a freeway segment, and the first-order hydrodynamic traffic flow theory is sufficient for illustrating the queue evolution. Daganzo (10-11) has proposed a behavioral theory for multilane freeway traffic flows, and argued that such a descriptive model is sufficient for development of computer programs.

Recently, Wong et al. (12) have extended the traditional LWR traffic theory (Lighthill and Whitham, (13); Richards, (14)) with the Lax-Friedrichs scheme, and claimed that their extended model can explain some complicate phenomenon that cannot be captured with the LWR model.

This study presents our recent work along the same line, that is, a first-order macroscopic traffic flow model for multiclass drivers. The model presented hereafter intends to overcome some limitations of the LWR model without using complex high-order formulations. The primary objective of this study, in fact, is similar to the recent work by Wong *et al.*, but with a different modeling methodology and a potentially more effective numerical method to solve our proposed multiclass traffic flow model. With a simple first-order formulation, our proposed model is capable of illustrating some vital freeway traffic dynamics such as the commonly observed oscillations of flow rate and density along a freeway segment over time, even without the disturbance of ramp flows and having uniform initial traffic conditions. The temporal and spatial variation of flow rate and density based on our proposed model will vary with different distributions of driving populations in the traffic stream.

TRAFFIC MODEL FOR MULTI-CLASS DRIVERS

For convenience of presenting the core logic, our proposed model is developed with the following two main assumptions:

- The effects of ramp flows, viewed as interactions between the mainline traffic stream and external environments, are not included in the formulations.

- Driving populations of each mainline traffic stream can be divided into several distinct classes, and their responses to the traffic condition are governing by the global freeway density, their own preferred free-flow speed, perceived jam density, and most importantly their unique speed-density relation.

Note that the existence of multiclass driving populations is evident from the commonly seen multiple platoons in the freeway traffic stream, where drivers with similar behavioral preferences and vehicle conditions tend to react similarly and travel in groups under the same traffic condition.

Thus, let u_0 be denoted as the free-flow speed, and ρ_m be the density, from the first order macroscopic traffic dynamics, the governing equations for the freeway traffic system can be written as

$$\frac{\partial \rho_i}{\partial t} + \frac{\partial(\rho_i u_i)}{\partial x} = 0 \tag{1}$$

If t and x use the units of $\Delta x / u_0$, and Δx . Under the assumption of having three classes of driving populations, one can present the supplementary traffic flow relations as follows:

$$u_i = v_{f,i}(1-\rho^{n_i}),\ \rho = \sum_{i=1}^{3} \rho_i \tag{2}$$

Where $v_{f,i}$ and n_i are the free-flow speed and the index of speed-density relation for the i-*th* class of drivers. Note that when drivers in each class share the same free-flow speed, it indicates that there exists one class of drivers who share the same fundamental relationship (1). When the parameter is set as 1, it means that a linear Greenshield model is used to reflect the speed-density relation (15).

By using the normalized optimal density, b_i with respect to the jam density (at b_i , the flow rate equals the roadway capacity), it is evident that the flow derivative with respect to density should be vanished at $\rho_i = b_i$. Hence, we can have the expression for b_i as a function of n_i :

$$b_i^{n_i} = \frac{1}{n_i + 1} \tag{3}$$

Note that for three classes of driving populations, the governing equations should generally have three characteristic values corresponding to their respective characteristic directions along which infinitesimal disturbances propagate (16). To ensure that the characteristic values are real, the supplementary relations should be properly selected. Under properly defined initial and boundary conditions, one shall be able to have solutions for the governing equation regardless of the employed numerical method. In this proposed multiclass freeway traffic model, for convenience, we assume that the free-flow speed has a priori assigned value that varies with the index of speed-density relationship.

To evaluate the properties of our proposed model, we have solved it with the Total Variation Diminishing (TVD) method due to Yee-Roe-Davis (18-20), and presented the numerical results of several experimental traffic scenarios in the ensuing two sections.

NUMERICAL SOLUTIONS FOR THE PROPOSED MODEL

The aforementioned governing equations for our proposed multiclass traffic flow model can be written in the following vector form

$$\frac{\partial \boldsymbol{\rho}}{\partial t} + \frac{\partial \mathbf{F}(\boldsymbol{\rho})}{\partial x} = 0 \tag{4}$$

where the density vector $\boldsymbol{\rho} = (\rho_1, \rho_2, \rho_3)^T$ is accompanied with its corresponding flux $\mathbf{F} = (F_1, F_2, F_3)^T$ whose components are given by

$$\begin{cases} F_1 = v_{f,1}\rho_1(1-\rho^{n_1}) \\ F_2 = v_{f,2}\rho_2(1-\rho^{n_2}) \\ F_3 = v_{f,3}\rho_3(1-\rho^{n_3}) \end{cases} \tag{5}$$

where the superscript T denotes the matrix transposition. According to the velocity measure given in the foregoing section, for the flux component F_2, we have $v_{f,2}$. Thus, the Jacobian matrix for equation (4) is

$$\mathbf{A} = \begin{pmatrix} \frac{\partial F_1}{\partial \rho_1} & \frac{\partial F_2}{\partial \rho_2} & \frac{\partial F_3}{\partial \rho_3} \\ \frac{\partial F_2}{\partial \rho_1} & \frac{\partial F_2}{\partial \rho_2} & \frac{\partial F_2}{\partial \rho_3} \\ \frac{\partial F_3}{\partial \rho_1} & \frac{\partial F_3}{\partial \rho_2} & \frac{\partial F_3}{\partial \rho_3} \end{pmatrix} = \begin{pmatrix} a_{11} & a_{12} & a_{13} \\ a_{21} & a_{22} & a_{23} \\ a_{31} & a_{32} & a_{33} \end{pmatrix} \tag{6}$$

for which the characteristic equation is

$$\lambda^3 + c_1\lambda^2 + c_2\lambda + c_3 = 0 \tag{7}$$

with the coefficients

$$c_1 = -\mathrm{tr}\mathbf{A},\ c_2 = A_{11} + A_{22} + A_{33},\ c_3 = -[a_{11}A_{11} + a_{12}A_{12} + a_{13}A_{13}] \tag{8}$$

Note that $\mathrm{tr}\mathbf{A}$ means the trace of matrix $\mathbf{A}$, and A_{ij} is the algebraic complement of the elements a_{ij} of the determinant $|\mathbf{A}|$, respectively. Expressing p and p_1 in terms of the coefficients in equation

$$p = \frac{c_2}{3} - \left(\frac{c_1}{3}\right)^2,\ p_1 = \frac{1}{2}\left[c_3 - c_2\left(\frac{c_1}{3}\right) + 2\left(\frac{c_1}{3}\right)^3\right] \tag{9}$$

for $p_1^2 + p^3 < 0,$ and $p < 0$, from the handbook of mathematics (12), the three real roots of the characteristic equation can be given by

$$y_k = \frac{1}{3}\mathrm{tr}\mathbf{A} + 2s^{1/3}\cos(\theta + 2(k-1)\pi/3),\ \text{for}\ k = 1,2,3 \tag{10}$$

where s and θ are given by

$$s = \sqrt{-p^3}\,,\ \theta = \frac{1}{3}\cos^{-1}(-p_1 / s) \tag{11}$$

For convenience of using the TVD method described below, the roots are arranged in a growing order. That means the characteristic values of the traffic system can be written as

$$\lambda_1 = \min(y_1, y_2, y_3),\quad \lambda_3 = \max(y_1, y_2, y_3),\quad \lambda_1 \le \lambda_2 \le \lambda_3 \tag{12}$$

With the Jacobian matrix, we obtain the right characteristic matrix in the following form:

$$\mathbf{R} = [\mathbf{r}_1, \mathbf{r}_2, \mathbf{r}_3] = \begin{pmatrix} r_{11} & r_{12} & r_{13} \\ r_{21} & r_{22} & r_{23} \\ r_{31} & r_{32} & r_{33} \end{pmatrix} \tag{13}$$

Where the elements can be written as

$$\begin{cases} r_{11} = 1,\ r_{21} = \frac{-a_{21}(a_{33}-\lambda_1)+a_{31}a_{23}}{\Delta_1},\ r_{31} = \frac{-a_{31}(a_{22}-\lambda_1)+a_{21}a_{32}}{\Delta_1} \\ r_{22} = 1,\ r_{12} = \frac{-a_{12}(a_{33}-\lambda_2)+a_{32}a_{13}}{\Delta_2},\ r_{32} = \frac{-a_{32}(a_{11}-\lambda_2)+a_{12}a_{31}}{\Delta_1} \\ r_{33} = 1,\ r_{13} = \frac{-a_{13}(a_{22}-\lambda_3)+a_{23}a_{12}}{\Delta_3},\ r_{23} = \frac{-a_{23}(a_{11}-\lambda_3)+a_{13}a_{21}}{\Delta_3} \end{cases} \tag{14}$$

in which

$$\begin{cases} \Delta_1 = (a_{22} - \lambda_1)(a_{33} - \lambda_1) - a_{23}a_{32} \\ \Delta_2 = (a_{33} - \lambda_2)(a_{11} - \lambda_2) - a_{31}a_{13} \\ \Delta_3 = (a_{11} - \lambda_3)(a_{22} - \lambda_3) - a_{12}a_{21} \end{cases} \tag{15}$$

The reverse of $\mathbf{R}$ is denoted by $\mathbf{L} = (\mathbf{l}_1, \mathbf{l}_2, \mathbf{l}_3)^T$. With these notations, according to the TVD algorithm proposed by Yee-Roe-Davis, and expressing the time level as m, we have

$$\boldsymbol{\rho}_j^{m+1} = \boldsymbol{\rho}_j^{m} - \omega(\hat{\mathbf{F}}_{j+1/2} - \hat{\mathbf{F}}_{j-1/2}) \tag{16}$$

where $\omega (= \frac{\Delta t}{\Delta x})$ is the ratio of time to spatial intervals, and

$$\begin{cases} \hat{\mathbf{F}}_{j+1/2} = \frac{1}{2}[\mathbf{F}(\boldsymbol{\rho}_j) + \mathbf{F}(\boldsymbol{\rho}_{j+1}) + \sum_{k=1}^{3} \psi_{k,j+1/2}\mathbf{r}_{k,j+1/2}] \\ \psi_{k,j+1/2} = -\frac{1}{\omega}[(\omega\lambda_{k,j+1/2})^2 g_{k,j+1/2} + Q_k(\omega\lambda_{k,j+1/2})(\alpha_{k,j+1/2} - g_{k,j+1/2})] \end{cases} \tag{17}$$

and

$$\begin{cases} \alpha_{k,j+1/2} = l_{k,j+1/2}(\boldsymbol{\rho}_{j+1} - \boldsymbol{\rho}_j) \\ g_{k,j+1/2} = \min\mathrm{mod}(\alpha_{k,j-1/2}, \alpha_{k,j+1/2}, \alpha_{k,j+3/2}) \end{cases} \tag{18}$$

$Q_k(z)$ is the coefficient of viscous term, which has the form

$$Q_k(z) = \begin{cases} |z|, & \text{for} \quad |z| \geq \varepsilon_k \\ (z^2 + \varepsilon_k^2)/2\varepsilon_k, & \text{Otherwise} \end{cases} \tag{19}$$

with the parameter ε_k. While the minimum modification function is given by

$$\min\mathrm{mod}(z_1, z_2, z_3) = \begin{cases} \operatorname{sgn} z_1 \cdot \min(|z_1|, |z_2|, |z_3|), \\ \qquad \text{if} \quad \operatorname{sgn} z_1 = \operatorname{sgn} z_2 = \operatorname{sgn} z_3 \\ 0. \qquad \text{Otherwise} \end{cases} \tag{20}$$

where $\operatorname{sgn} z$ is the sign function whose value is 1,0, or -1, if z is positive, zero, or negative. The minimum modification function provides monotonic treatment for the numerical solution.

NUMERICAL RESULTS AND DISCUSSIONS

The section presents the numerical solutions of the above the multi-class model based on three classes of driving populations. Initial parameters for performing the numerical analyses are summarized below:

- Three modes, distinguished by their ratios to the optimal density, have been taken into account in the numerical simulation and are presented in Table 1. Note that the global density is uniform but defined as the sum of densities for all driving classes. The initial distribution of ρ_1 was performed with a computer-based random generator from an Erlang process of order 5 as shown in Figure 1. The initial distributions of the 2-*nd* and the 3-*rd* classes are assigned by using parameter β defined in Table 1.
- The free-flow speed of k-*th* class is given by the expression in Table 1. The expression implies that the road capacity is a constant for each class of drivers, and the free-flow speed corresponds to an optimal density 0.5.
- The parameters of speed-density relations $(n_i, i = 1,2,3)$ for these three driving classes are evaluated by using equation (3), where the speed unit u_0 is set as a unity.
- The parameters $(\varepsilon_k, k = 1,2,3)$ appear in Q_k were chosen as 0.025 at which the numerical viscous effect is negligible.

Note that under the assumption of having a uniform initial global density, the traditional LWR traffic model will naturally lead to the conclusion of always having a time-independent global density ρ. This is certainly inconsistent some field observations. However, with our proposed model, as shown in the ensuing presentation of numerical results, seems to offer the potential to better explain the traffic dynamics such as the observable oscillations of traffic densities and flow rates on freeway segments even without including the disturbance from ramp-flows (6).

Table 2 represents the time averaged and root of mean square (rms) values of the data sequences for flow rate and densities occurred at *x*=100. The first column indicates those five cases in the numerical experiment. The time averaged flow rate is seen to be mode dependent, but the peak value of the averaged flow rate is found to have a peak when the initial density (ID) is 0.5.

The rms value is of course a measure of oscillation magnitude for the simulated data. The rms of flow rate can be seen from the 3-*rd* column of Table 2. It varies with the mode choice, and has a largest value in an order of about 10^{-3} as the ID is 0.3. However, the mode dependence of rms value is more significant when ID value is less than 0.5. For example, for density 0.3, from the 3-rd row of Table 1, the rms of flow rate under mode I is 1.81×10^{-3}; for density 0.4 it equals 1.93×10^{-3}. But under mode III, their rms value is 2.32×10^{-3}. The rms of flow rate approaches its *minima* as ID value is set at 0.5. The rms of global density is, in general, less than that of flow rate (see column 4 of Table 1). However, from the data shown in the 5-*th* and 6-*th* columns, it is clear that the rms value of the fractional density is almost mode independent.

The evolution of global density at *x*=100 for ID being assigned as (a) 0.3, (b) 0.5, and (c) 0.7 is given in Figure 2, in which the dash-dotted, dashed, and solid curves correspond to modes I, II, and III, respectively. Clearly, density oscillations happen as ID is taken as 0.3, at which the oscillating magnitude is comparable to that of the initial waves. For over saturated traffic, the initial irregular waves are largely suppressed. These oscillations come from the initial heterogeneous distributions of those densities of multi-driver classes, even though the initial global density is set to be uniform along the entire freeway segment.

The evolution of densities at *x*=100 for the first and second classes for ID being assigned as (a) 0.3, (b) 0.5, and (c) 0.7 can be viewed from Figure 3, where all curves exhibit similar relations between different modes as in Figure 2. The variation of vehicular density for the second class shows a reverse trend to the variation of the first class. Thus, when a valley of the 1-*st* class density curve occurs, there exists a peak density value for the 2-*nd* class. Such coherent traffic states are due to the assumed initial conditions. For ID being assigned as 0.5, the choice of different modes has little impact on evolution of the density pattern.

To show that the proposed model has the property of capturing the density and flow rate oscillation, we have employed power spectra recommended in the literature (21) to analyze the numerical results. As given in Figures 4 (a) and (b), one can observe the primary oscillating frequencies from the exhibited patterns. The results in Figure 4 correspond to those in Figures 2, and 3, and the data is selected at x=100 for mode III. The values of the two primary frequencies are given in Table 3. Clearly, the choice of different modes has some impacts on the primary frequencies when the ID is set to be 0.3. It is the main frequency with a larger power spectrum that dominates the oscillating performance.

From Table 3, it can be seen that when the initial density is less than 0.6, the two primary frequencies decrease with the initial density. For ID at 0.7, it has the same primary frequencies as that in the case which has the initial density of 0.6. For example, for Mode I, from the 2-*nd* column of Table 3 where ID is 0.3, the primary frequencies f_1, and f_2 have the values of 7.58×10^{-3}, and 1.834×10^{-2}, respectively.

Note that by setting the dimensional value of Δx at 180m, the free-flow speed as 30m/s, and the time unit to be 6s, in the case of ID equal to as 0.3, the dimensional primary periods of traffic oscillation are 13.32mn, and 5.45mn (*i.e.* $6/f_1/60$, and $6/f_2/60$). Such a period of traffic oscillation can be found in the real-world data from Paris (22), for Germany (6), and San Francisco (1).

To see traffic flow pattern in terms of global density, the contours of traffic density under mode III for the initial density of (a) 0.3, (b) 0.5, and (c) 0.7 are illustrated in Figure 4. These patterns indicate not only that the evolution of solid curves in Figure 2 are really observed at *x*=100, but also that the traffic wave propagates according to the orientation of the given density structures. These contours, labeled by the initial density, can better capture the traffic pattern. One can also see from Figure 4 that the traffic waves propagate downward along the steep and diminished directions (see, parts (a) and (b) of Figure 4). However, the propagation direction for the case of density equal to 0.7 is clearly going upward (see part (c) of Figure 4). These contours exhibit a dense spacing at the early stage of density evolution, and become coarse at the later stage. The evident wrinkles and local structures occur particularly for the cases of density equal to 0.5, and 0.7, as shown in parts (b) and (c) of Figure 4.

In summary, the numerical results shown in the above figures and tables are consistent with some real-world observations (1, 6, 22), and offer a plausible explanation for observed traffic density oscillation on freeway segments without external disturbances. Our proposed multi-class macroscopic model with its simple first-order relation seems capable of illustrating such vital traffic flow dynamics.

CONCLUSIONS

The paper has presented a first-order multiclass macroscopic traffic flow model and its numerical solutions. The proposed model uses the free-flow speed and the speed-density relation to characterize each class of drivers. Numerical analyses with the TVD method have indicated that by taking into account the behavioral discrepancy of various driving populations our proposed model is capable of illustrating some vital traffic flow dynamics, i. e., *if the density is less than its optimal density, a freeway segment with an initially uniform global density and flow rate may exhibit a pronounced oscillating pattern even without any ramp flow disturbance*. This is likely due to the heterogeneous distributions of different driving populations who may react differently under identical traffic conditions.

It, however, should be mentioned that the impact of multiclass driving populations on the traffic dynamics is a quite complex issue, and much remains to be explored along this research direction. Our on-going work has focused on the interrelations between the number of driving classes and the dynamic properties of the resulting traffic flows. The impact of ramp flows on the stability and the variability of the global traffic patterns will also be explored.

ACKNOWLEDGEMENTS

The authors would like to thank the reviewers of this manuscript as they have provided invaluable comments and suggestions for our revision work.

REFERENCES

1. Zhang, H. M.(1999). Analyses of the stability and wave properties of a new continuum theory.*Transp. Res. Part B: Methodol*., 33, 399-415.
2. Helbing, D., Hennecke, A., Shvetsov, V. and Treiber, M. (2001). MASTER: macroscopic traffic simulation based on gas-kinetic, non-local traffic model.*Transp. Res. Part B: Methodol.*, 35, 183-211.
3. Helbing, D., Batic, D. Schonholf, M and Treiber, M. (2002). Modeling widely scattered states in synchronized traffic flow and possible relevance for stock market dynamics. *Physica A*, 303, 251-260.
4. Nagatani, T. (2000) Traffic behavior in mixture of different vehicles. *Physica A*, 284, 405-420.
5. Hoogendoorn, S. P. And Bovy P. H. L. (2000). Continuum modeling of multiclass traffic flow. *Transp. Res. Part B: Methodol.*, 34, 123-146.
6. Kuhne, R. D. and Michalopoulos P. (2001). Continuum flow models. Chapter 5 of Traffic Flow Theory. see, http://www-cta.ornl.gov/cta/research/trb/tft.html.
7. Daganzo, C. F. (1995). Requiem for second order approximation of traffic flow. *Transp. Res. Part B: Methodol.*,24(4), 277-286.
8. Zhu, Z., and Wu, T. (2003). A two phase fluid model for freeway traffic and its application to simulate the evolution of solitons in traffic. ASCE, *J. Transportation Engineering*, to appear.
9. Cassidy, M.J. and Mauch, M. (2001). An observed traffic pattern in long freeway queues. *Transp. Res. Part A* 35, 143-156.
10. Daganzo, C. F. (2002). A behavioral theory of multi-lan traffic flow. Part I: Long homogeneous freeway sections. *Transp. Res. Part B: Methodol*., 36, 131-158.
11. Daganzo, C. F. (2002). A behavioral theory of multi-lan traffic flow. Part II: Merges and the onset of congestion. *Transp. Res. Part B: Methodol.*, 36, 159-169.
12. Wong, G. C. K., Wong, S. C. (2002). A multi-class traffic flow model-an extension of LWR model with heterogeneous drivers. *Transp. Res. Part A*, 36, 827-841.
13. Lighthill, M. J., and Whitham G.B. (1955). On kinematic waves; II. a theory of traffic flow on long crowded roads. *Proc., Roy. Soc. Ser*. 229A, 317-345.
14. Richards, P. I. (1956). Shock waves on the freeway. Operations Res., 4, 42-51.
15. Greenshields, B. D. (1934). A study of traffic capacity. Proceedings of the Highway Research Board 14, 448-477.
16. Wang L. X. (1979). Handbook of Mathematics. Publisher of Higher Education, Beijing, 80-100.
17. Glimm, J. (1965). Solutions in the large for nonlinear hyperbolic systems of equations. *Comm. Pure Appl. Math*., 18, 697-715.
18. Davis, S. F. (1988).Simplified second- order Godunov- type methods. *J. Sci. Statist Comput.*, SIAM, No. 9, 445-473.
19. Roe, P. C. (1981). Approximate Riemann solvers, parameter vectors, and difference schemes. *J. Comput. Phys*., 43, 357-372.
20. Yee, H. C. (1987). Construction of explicit and implicit symmetric TVD schemes and their applications. *J. Comput Phys*., 68, 151-179.
21. Zhu, Z., Yang, H. (2002). Discrete Hilbert transformation and its application to estimate the wind speed in Hong Kong. *J. Wind Eng. Ind. Aerodynamics*. 90, 9-18.
22. Papageorgiou, M., Blosseville, J. M. and Hadj-Salem, H., (1989), Macroscopic modeling of traffic flow on the boulevard Peripheique in Paris, *Transp*. Res. *Part B: Methodol.*, 23(1), 29-47.

NOMENCLATURE

A	=Jacobian matrix;
|A|	= determinant of matrix A;
A_{ij}	=algebraic complements for matrix element a_{ij} ;
a_{ij}	=elements of A;
b_i	= ratio of optimal to jam density;

c_1, c_2, c_3	=coefficients of characteristic equations;
F	=flow vector;
g_k	= given by Eq(18);
L	=left characteristic matrix;
l_k	=left characteristic vector for root λ_k ;
n_i	=index of speed-density relation, see Eq. (2);
p	= intermediate coefficients, see Eq. (9) ;
p_1	= see Eq(9);
Q_k	=coefficients of numerical viscous term;
q	= flow rate (=F_1+ F_2 +F_3) ;
q_0	= road capacity;
R	= right characteristic matrix ;
r_k	=right characteristic vector for root λ_k ;
rms	= root mean square;
s	=defined in Eq.(11)
t	= time;
tr	=trace, i.e. the summation of the diagonal elements of a matrix;
u_i	= defined by Eq.(2);
$v_{f,i}$	= free speed for class *I*;
y_k	=roots of characteristic equation.
x	= space;
z	= intermediate variable.
Greek Symbols	
α_k	= given by Eq. (18);
Δ_k	= given by Eq. (15);
λ_k	=k-th characteristic value;
ω	=ratio of time to spatial step;
ψ_k	= given by Eq. (17)
$\boldsymbol{\rho}$	= density vector ;
ρ	= traffic density;
ρ_k	=fractional density for drivers' class *k;*
ρ_m	= jam density;
Superscripts	
m	= time level;
T	= transposition of a matrix
Over bar	= means time average.

List of tables

List of Figures

Table 1. The initial parameters used in numerical simulation

b_k	Mode I: 0.49, 0.47, 0.45, for k=1,2,3 Mode II: 0.50, 0.48, 0.46, for k=1,2,3 Mode III: 0.52, 0.50, 0.48, for k=1,2,3
$v_{f,k}$	$=0.25/[b_k(1-b_k^{n_k})]$
n_k	Evaluated by Eq.(3)
ε_k	0.025, for k=1,2,3
β	$=\rho_2/(\rho_2+\rho_3)=75\%$, for t=0.

Table 2. The average flow rate and rms values of flow rate and densities for several $\rho|_{t=0}$ at $x=100$ under different modes.

$\rho\|_{t=0}$	$\bar{q}$	σ_q	σ_ρ	σ_{ρ_1}	σ_{ρ_2}
			Mode I		
0.3	0.882	1.81×10^{-3}	8.05×10^{-4}	6.93×10^{-3}	6.38×10^{-3}
0.4	0.978	5.02×10^{-4}	2.68×10^{-4}	1.01×10^{-2}	8.10×10^{-3}
0.5	0.996	1.11×10^{-4}	0.70×10^{-4}	1.35×10^{-2}	1.04×10^{-2}
0.6	0.936	3.94×10^{-4}	2.94×10^{-4}	1.66×10^{-2}	1.32×10^{-2}
0.7	0.803	6.33×10^{-4}	3.79×10^{-4}	1.61×10^{-2}	1.29×10^{-2}
			Mode II		
0.3	0.868	1.93×10^{-3}	8.53×10^{-4}	6.84×10^{-3}	6.32×10^{-3}
0.4	0.973	5.99×10^{-4}	3.22×10^{-4}	1.00×10^{-2}	8.06×10^{-3}
0.5	0.998	0.67×10^{-4}	0.45×10^{-4}	1.36×10^{-2}	1.03×10^{-2}
0.6	0.945	3.85×10^{-4}	2.76×10^{-4}	1.66×10^{-2}	1.32×10^{-2}
0.7	0.816	6.31×10^{-4}	3.78×10^{-4}	1.62×10^{-2}	1.30×10^{-2}
			Mode III		
0.3	0.838	2.32×10^{-3}	10.2×10^{-4}	6.86×10^{-3}	6.43×10^{-3}
0.4	0.959	8.39×10^{-4}	4.57×10^{-4}	0.99×10^{-2}	8.20×10^{-3}
0.5	0.999	0.34×10^{-4}	0.18×10^{-4}	1.36×10^{-2}	1.02×10^{-2}
0.6	0.960	3.54×10^{-4}	2.33×10^{-4}	1.66×10^{-2}	1.31×10^{-2}
0.7	0.840	6.11×10^{-4}	3.89×10^{-4}	1.63×10^{-2}	1.31×10^{-2}

Table 3. The primary frequency and period of the density sequence at $x=100$

$\rho \|_{t=0}$	0.3	0.4	0.5	0.6	0.7
			Mode I		
f_1	7.508×10^{-3}	6.675×10^{-3}	5.008×10^{-3}	4.175×10^{-3}	4.175×10^{-3}
f_2	1.834×10^{-2}	1.502×10^{-2}	1.335×10^{-2}	1.002×10^{-2}	1.085×10^{-2}
			Mode II		
f_1	7.508×10^{-3}	6.675×10^{-3}	5.008×10^{-3}	4.175×10^{-3}	4.175×10^{-3}
f_2	1.752×10^{-2}	1.502×10^{-2}	1.252×10^{-2}	1.002×10^{-2}	1.002×10^{-2}
			Mode III		
f_1	6.675×10^{-3}	6.675×10^{-3}	5.008×10^{-3}	4.175×10^{-3}	4.175×10^{-3}
f_2	1.669×10^{-2}	1.502×10^{-2}	1.252×10^{-2}	1.002×10^{-2}	1.002×10^{-2}

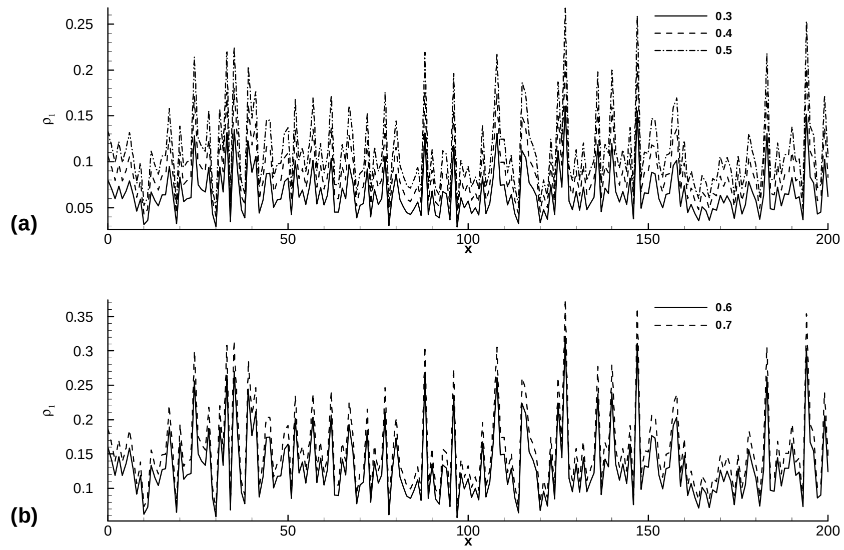

Figure1. Initial distribution of density of trucks which is given by a computer based random generator regarding Erlang process with order 5.

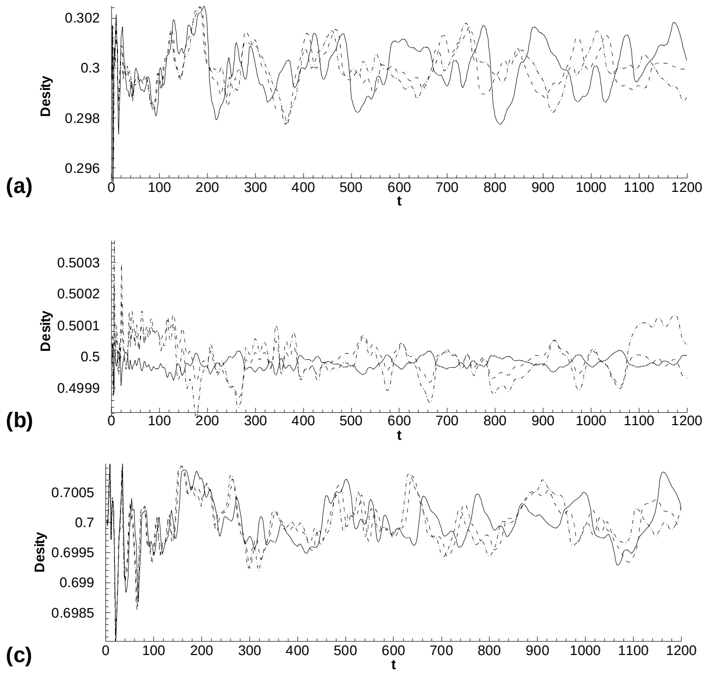

Figure 2. Evolution of global densities for freeway traffic for initial density assigned as (a) 0.3, (b) 0.5, and (c) 0.7 under diffrent modes.

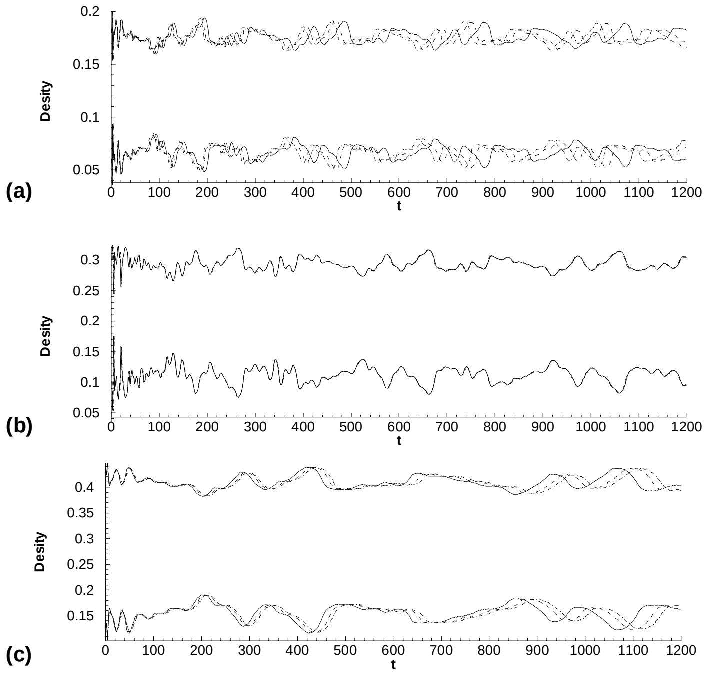

Figure 3. Evolution of densities of the first and second classes for freeway traffic for initial density assigned as (a) 0.3, (b) 0.5, and (c) 0.7 under different modes.

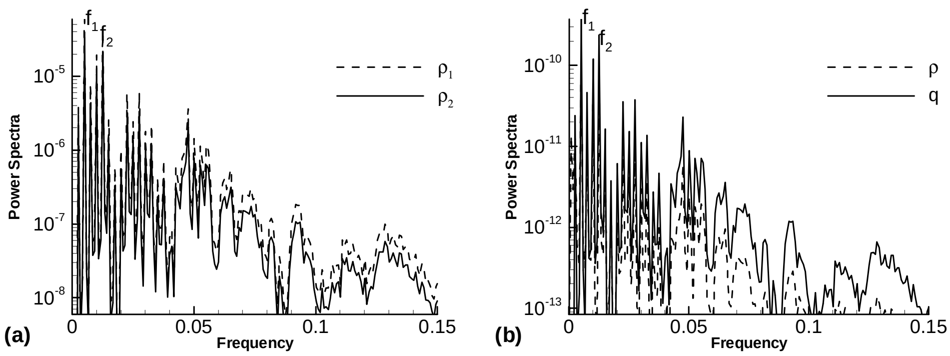

Figure 4. Power spectra of densities and flow rate for the case of initial density 0.5 for the three classes under mode III.

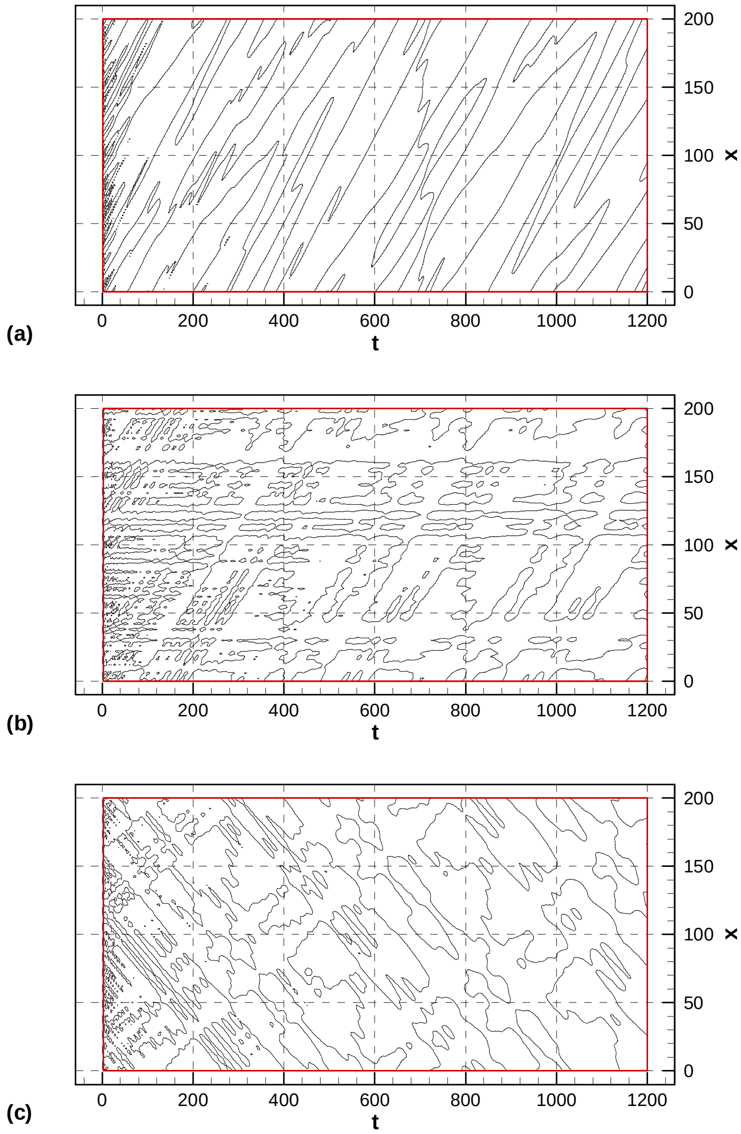

Figure 5. Contours of global density, where the initial densities (a) 0.3, (b) 0.5, and (c) 0.7 are used in the labeling contours under mode III.